FULL PAPER

# Plasmonic Gradient Effects on High Vacuum Tip-Enhanced Raman Spectroscopy

*Mengtao Sun,\* Zhenglong Zhang, Li Chen, Shaoxiang Sheng, and Hongxing Xu*

Experimental evidence is given of the breakdown of Raman selection rules in high vacuum tip-enhanced Raman spectroscopy (HV-TERS), where molecular Raman-active, IR-active, and overtone modes are simultaneously observed in situ, due to the strong tip-enhanced near-field gradient effects. Theoretical calculations firmly support our experimental multipole vibrational observation, and the ratio of the near-field gradient term over electric field term is dependent on both the ratio of $\frac{\partial E_{\beta\gamma}}{\partial r}/E_\beta$ and the ratio of $A_{\alpha\beta\gamma}/\alpha_{\alpha\beta}$, which are dependent on the physical structure of TERS and the molecular structure, respectively, in HV-TERS. When the molecule is symmetric along the tip axis, the strongest near-field gradient effect in HV-TERS can be obtained. These experimental findings can promote an understanding of the unexpected "additional Raman peaks" in HV-TERS and provide a promising technique for ultrasensitive molecular spectroscopy.

## 1. Introduction

Tip-enhanced Raman spectroscopy (TERS)[1–14] is a high-sensitivity optical analytical technique with nanoscale resolution beyond the diffraction limit of light. As a plasmon antenna controlled by tunneling current or bias voltage, a sharp metal tip is used to create a "hot site" to excite the localized surface plasmons and consequently enhance the electromagnetic field and Raman signals in the vicinity of the tip apex. In order to conduct spectral measurements that are sensitive to ambient conditions for a variety of specimens, the use of an ultra-high vacuum (UHV) environment is mandatory.[10,12] To obtain higher efficiency of collecting Raman signals, the objective had been put into the vacuum chamber and near the tip and the substrate in our novel designed high vacuum TERS (HV-TERS).[13]

TERS is mainly applied in combination with linear optical processes in Raman, but the strong field enhancements involved can also induce non-linear optical processes, such as second-harmonic generation (SHG),[15] and hyper-Raman.[16,17] Very recently, multiple vibrational modes[12] and electric field gradient effects[11,18] have been observed experimentally in TER spectra in UHV and HV environments, respectively. Physically,

Prof. M. Sun, Dr. Z. Zhang, L. Chen, S. Sheng,
Prof. H. Xu
Beijing National Laboratory for
Condensed Matter Physics
Institute of Physics
Chinese Academy of Sciences
PO Box 603–146, Beijing, 100190, PR China
E-mail: mtsun@aphy.iphy.ac.cn

these are attributed to the higher order terms of Hamiltonian for Raman spectra. The multiple vibrational modes and electric field gradient are different names, but reflect two aspects of higher order terms of Hamiltonian. For a molecule placed in an inhomogeneous electromagnetic field, the Hamiltonian for Raman spectra can be written as,[19]

$$H = \left( \alpha_{\alpha\beta} E_\beta + \frac{1}{3} A_{\alpha\beta\gamma} \frac{\partial E_{\beta\gamma}}{\partial r} \right) E_\alpha$$
$$+ \frac{1}{3} \left( A_{\gamma,\alpha\beta} E_\gamma + C_{\alpha\beta,\gamma\delta} \frac{\partial E_{\gamma\delta}}{\partial r} \right) \frac{\partial E_{\alpha\beta}}{\partial r} + \cdots$$

(1)

where $\alpha_{\alpha\beta}$, $A_{\alpha\beta\gamma}$ and $C_{\alpha\beta,\gamma\delta}$ and are the electric dipole–dipole polarizability, the electric dipole–quadrupole polarizability and the electric quadrupole–quadrupole polarizability, and $E_\alpha$ and $\frac{\partial E_{\alpha\beta\gamma}}{\partial r}$ are the external electric field and external electric field gradient, respectively. The ratio of the intensity of multiple Raman over dipole Raman is dependent on the ratio of $\left( A_{\alpha\beta\gamma} \frac{\partial E_{\beta\gamma}}{\partial r} \right)/\left( \alpha_{\alpha\beta} E_\beta \right)$. More detailed, $\left( \frac{\partial E_{\beta\gamma}}{\partial r} \right)/\left( E_\beta \right)$ and $\left( A_{\alpha\beta\gamma} \right)/\left( \alpha_{\alpha\beta} \right)$ are dependent on the palsmonic properties of TERS and the molecular property of polarizability, respectively. Till now, near field gradient effect is a largely unexplored territory in HV-TERS. **Figure 1** shows our home-made HV-TERS, and the qualitative $E_\alpha$, $\frac{\partial E_{\alpha,\beta\gamma}}{\partial r}$ and their ratio for palsmonic properties of TERS (detailed calculations will be shown in the next section).
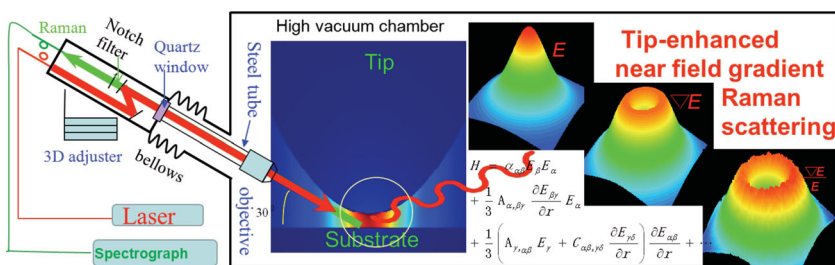
Fermi resonance, a overtone or a combination modes appearing in the vibrational spectra by gaining intensity from a fundamental mode,[20] were frequently found in IR or Raman spectra in symmetric triatomic molecules such as $CO_2$ and $CS_2$.[21–23] Darling–Dennison resonance,[24] two degenerated first overtone modes perturbed each other and gain the Raman intensity, were also been observed in Raman spectra, such as $H_2O$.[25] In HV-TERS, Fermi resonance and Darling–Dennison resonance have been observed experimentally,[11,14] due to the near field gradient effect.

Until now, there is no completely experimental report on the nonlinear effects in HV-TERS, including both the optical nonlinear and molecular nonlinear effects simultaneously. In this paper, we report experimentally report both plasmonic nonlinear and molecular nonlinear vibrational effects in HV-TERS of pyrazine adsorbed on Ag film. The vibrational mode of pyrazine with $B_u$ symmetry is the IR-active in IR spectra, and usually can not be observed in Raman spectra (IR-active is usually Raman-inactive). In our experiment, the vibrational

www.MaterialsViews.com
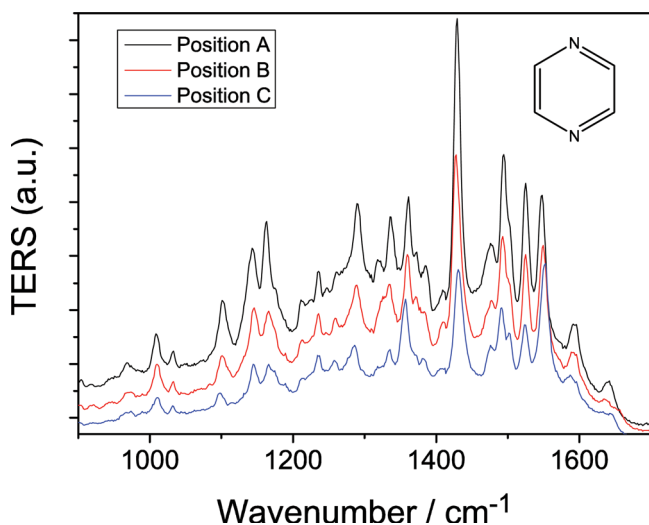
ADVANCED
OPTICAL
MATERIALS
www.advopticalmat.de

FULL PAPER

**Figure 1.** The home-made HV-TERS and plasmonic properties of electric field E, electric gradient $\left(\frac{\partial E_{\beta\gamma}}{\partial r}\right)$ and the ratio of $\left(\frac{\partial E_{\beta\gamma}}{\partial r}\right)/(E_\beta)$ in TERS.

modes with $B_u$ symmetry (IR-active modes) were also observed in HV-TERS, resulting from interaction between the electric dipole–quadrapole polarizabily and the electric field gradient. The IR-active modes resulted from electric gradient effect, the Raman-active modes, the overtone and the combinational modes resulted from Fermi resonance were all in situ observed simultaneously. These experimental findings can promote deep understanding of the unexpected "additional Raman peaks" in HV-TERS and provide a promising technique for ultrasensitive molecular spectroscopy.

## 2. Results and Discussion

### 2.1. The Near-Field Gradient Effect on HV-TER Spectra

The HV-TER spectra of pyrazine adsorbed on Ag film can be seen from **Figure 2**, which were reproducible at different positions. The signals from the decomposition of pyrazine and from the Ag substrate can be ignored in our HV system. Theoretical calculations revealed that molecules were standing on the substrate (see Figure S1 in Supporting Information), and their IR and Raman spectra of pyrazine adsorbed on the Ag film were shown in Figure S2 in SI. The Raman spectrum of pyrazine adsorbed on the Ag film can be considered as the
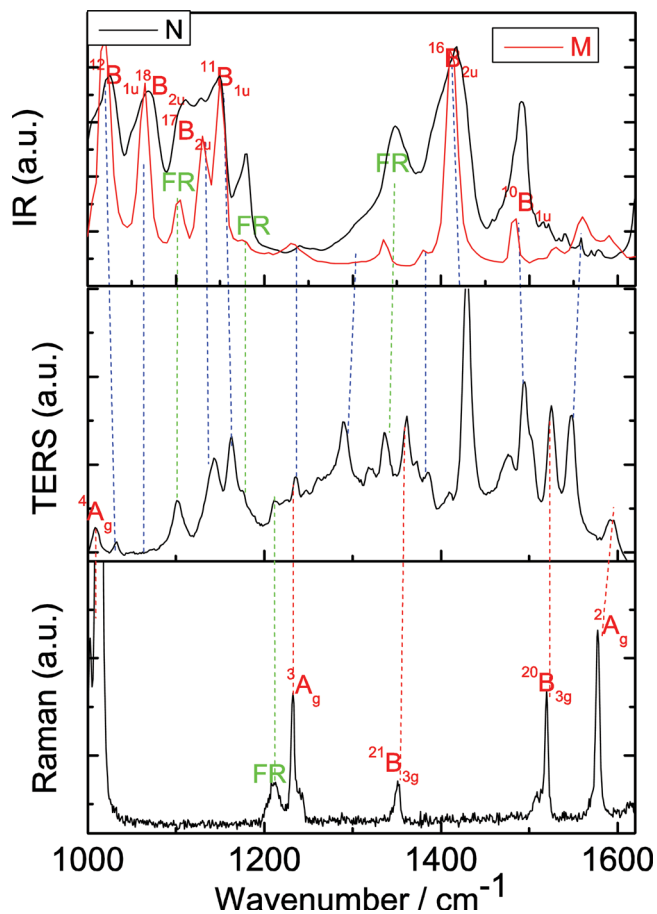
surface enhanced Raman scattering (SERS) spectrum. It is found that TER spectrum and simulated SERS spectrum are significantly different. Because of near field gradient effect in TERS, there are much more peaks (IR-active modes) in Figure 2 than that in SERS. The calculated SERS spectrum supported that additional peaks in TER spectra were not from the breaking of the symmetry induced by molecules interacting with the surface.

For assignments and comparisons, the Raman, IR spectra of pyrazine powder were also measured, see **Figure 3**. It was found that the HV-TER spectrum is significantly different from the Raman spectrum. Assignments of the Raman vibrational modes can be found in the literature.[26] Almost all the Raman modes of pyrazine powder can be observed in HV-TERS and there are many "additional" strongly enhanced modes in HV-TERS. There are several possible ways to interpret these additional peaks. They could be originated from the chemical enhancement, the IR-active modes, the overtone or combinational modes in HV-TERS. To identify the origin of these additional peaks, we measured the IR vibrational spectrum of the pyrazine powder



**Figure 2.** TER spectra of pyrazine at different positions of Ag substrate.



**Figure 3.** (a) the measured IR spectrum of pyrazine powder, (b) HV-TERS of pyrazine adsorbed on Ag film, and (c) Raman spectrum of pyrazine powder.

(black curve N in IR spectrum), and compared with the IR spectrum (red curve M) taken from ref. [27], which were measured with different method. The profiles of these IR spectra were different (interpretation can be seen in the literature,[27] but frequencies of their IR modes are the same. The assignments of the IR vibrational modes of pyrazine can be found in the literature.[26] Comparing the IR and HV-TER spectra, we find that some of the strongly enhanced vibrational peaks may be from the IR-active modes of pyrazine. The calculated strong IR peak at 1415 cm$^{-1}$ in Figure S2 strongly supported that the experimental strong vibrational peak around 1430 cm$^{-1}$ in TER spectrum in Figure 2 is the IR peak. Note the shift is from the tip influence, where Figure S2 is the calculated SERS spectrum without the tip effect. When compared TERS spectra with IR and Raman spectra of the powder, there are multiple frequency shifts of the peaks both to the blue and to the red. The origin may be the interactions among molecule, tip and substrate. The detailed shifts were listed in Table S1 in SI.

In the Raman and IR vibrational spectra of pyrazine powder, there are four nonlinear molecular vibrational peaks resulted from Fermi Resonance. The assignment of Fermi resonance peaks can be seen in the literature.[26] In HV-TERS, it is found that these Fermi resonance peaks can also be clearly observed in Figure 3. For example, the Fermi resonance peak at 1106 cm$^{-1}$ is perturbed with $^{18}B_{2u}$, where the peak at 1106 cm$^{-1}$ is the combinational modes of $^7A_u + ^{14}B_{2g}$ at 350 and 756 cm$^{-1}$, respectively. Detailed description on Fermi resonance can be seen from Section II in SI.

It is interesting to measure the SERS spectrum of pyrazine on the Ag substrate that used in HT-TERS, and compare the SERS spectrum with the TER spectra. In the SERS measurements, the system of the Ag nanoparticle and Ag film was used, because without the nanoparticles, the SERS spectra of pyrazine on the Ag film can not be observed. Another reason is the coupling between nanoparticles-film system is similar with the TERS system of tip and substrate. Recently, electromagnetic field redistribution in hybridized plasmonic particle-film system has been experimental and theoretical studied, and it is a better way to measure SERS spectra.[28,29] **Figure 4** demonstrates that without the influence of tip, the numbers of Raman

peaks in SERS are less than those in TER spectra. Furthermore, these Raman shifts still happened, due to the tip influence. It is found that some IR-active modes also be found in SERS, due to the coupling between particle, and the hybridized plasmonic gradient effect in the particle-film system. In our HV-TERS, the Ag substrate was prepared by evaporating, so the Ag substrate is roughness, which may be also one of factors for the observation of IR-active modes in HV-TER and SERS spectra. By comparing the TER spectra and SERS spectra in Figure 4, we can get advantages of HV-TERS. The molecular concentration in SERS is 10$^{-2}$ M; while it is 10$^{-4}$ M in HV-TER spectra, but the signals of Raman spectra TER in HV are significantly better than that in SERS, which clearly revealed the advantages of HV for the ultrasensitive spectral analysis. At the molecular concentration of 10$^{-4}$ M in SERS, the Raman signals were too weak to be observed.

These additional peaks in the SERS spectroscopy were recently interpreted as the fluctuating signals of the amorphous carbon.[30,31] By comparing our SERS and HV-TER spectra, we can exclude this issue. These "additional peaks" should result from the simultaneous combined contribution of electric field gradient and molecular multipolar polarizability.

## 2.2. The Theory of the Near Field Gradient Effect on HV-TERS

The first term in Equation (1) is the coupling among molecular polarizability, incident field and scattered field. The second term is the coupling among electric dipole-quadrupole polarizability, incident field and scattered field gradient. The third term is the coupling among the electric dipole–quadrupole polarizability, incident field gradient and scattered field. And the last term is coupling among electric quadrupole-quadrupole polarizability, incident field gradient and scattered field gradient.

Molecular vibrations belonging to the same irreducible representations as components of tensor $A_{\alpha\beta\gamma}$ may now become active alongside the normally active modes which are spanned by the same representations as those which span components of $\alpha_{\alpha\beta}$. The selection rules for four terms in Equation (1) can be obtained by the same manner in the following form,[32]

$$\Gamma \in \Gamma_\mu = \Gamma_\theta \qquad (2)$$

where $\Gamma$ is the irreducible representation. The IR-active modes are allowed when there is a moment, which transforms after the same irreducible representation as the vibrational mode.[29] For example, the $\mu_\alpha$ of IR at 1163 cm$^{-1}$ is $B_{2u}$ symmetry, and the $\theta_{\beta\gamma}$ is also of $B_{2u}$ symmetry. Then the irreducible representation of $A_{\alpha\beta\gamma}$ at 1163 cm$^{-1}$ is $A_{2g}$ symmetry, which is Raman actives, so it is called IR-active mode in HV-TER spectra.

To reveal the strong electric field gradient effect in HV-TERS, local electric field enhancement and electric field gradient were calculated using the finite element method, which is implemented in COMSOL software (version 4.2). The model of TERS system in the calculation is shown in **Figure 5**a. The radius of the tip apex was 25 nm and the angle between the tip axis and the incident light was set at 60°. The distance between tip and substrate is 1 nm. For the simplification in the calculation, the frequencies of incident field and the scattered field are equally.
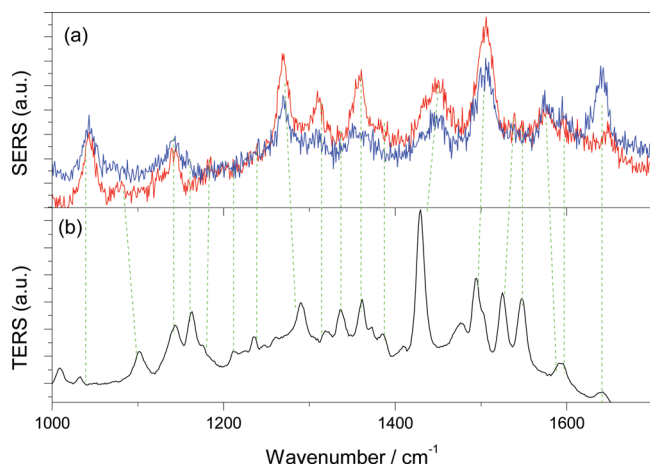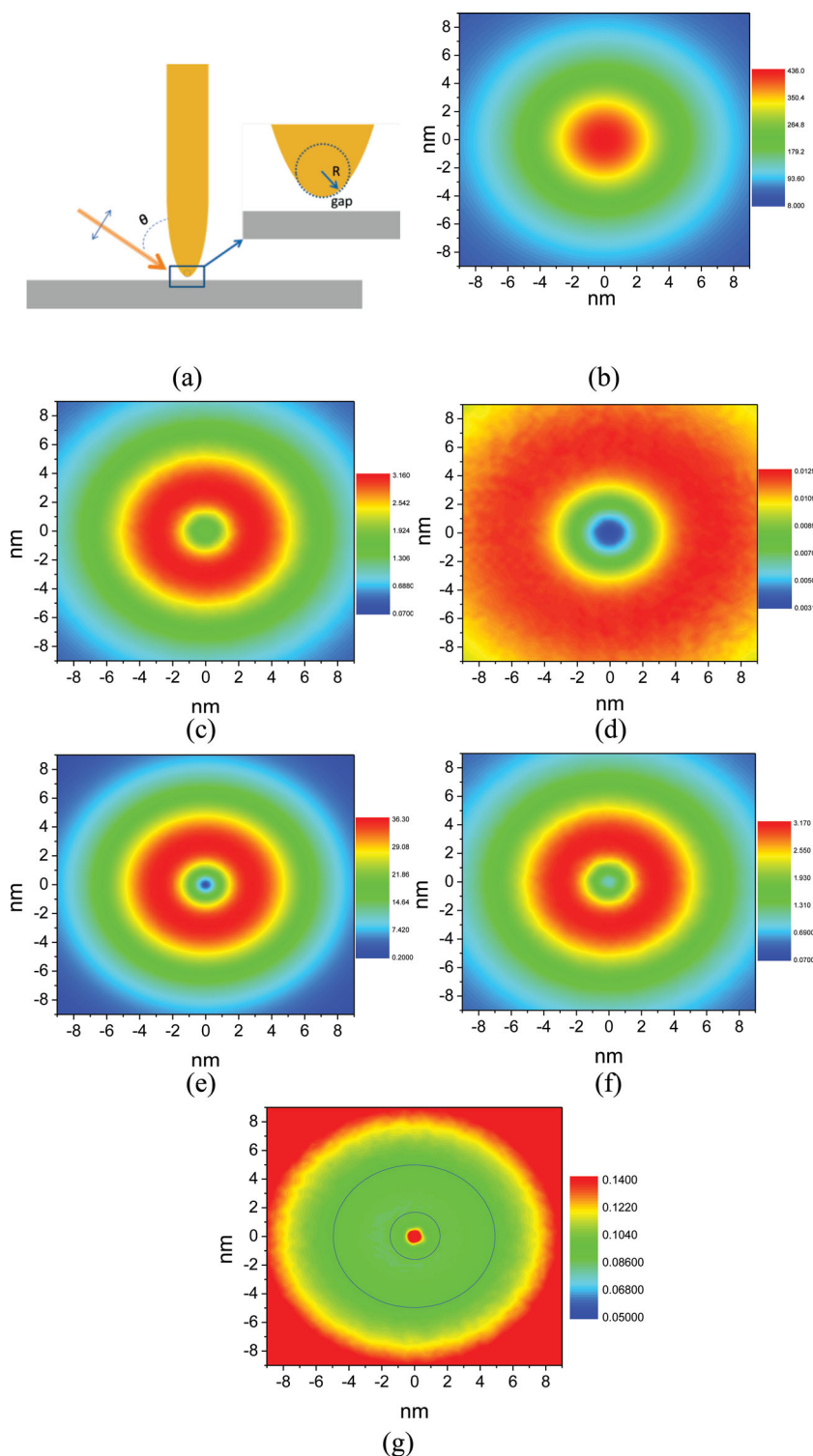


**Figure 4.** (a) SERS and (b) TER spectra of pyrazine.

www.MaterialsViews.com

ADVANCED
OPTICAL
MATERIALS
www.advopticalmat.de

FULL PAPER

**Figure 5.** (a) schematic diagram of the TERS setup used in calculations, (b) the electric field intensity along tip axis, (c) the electric field gradient intensity along tip axis (z axis), (d) the ratio of the electric field gradient over electric field intensity at 0.5 nm above the substrate, (e) the electric field intensity along the substrate at 0.5 nm above the substrate, (f) electric field gradient intensity along the substrate at 0.5 nm above the substrate. Note that the two-dimensional plane in the center of nanogap above the substrate is used to for the analysis of field distribution along the z axis and xy planes, since this two-dimensional plane is the detected region for Raman signals. Note that the unit of electric field intensity is V/m, and the unit of electric field gradient is V/m/au, where au is atomic unit.

Since pyrazine was standing on the substrate, the vibrations along the tip and along the substrate are two mainly different kinds of vibrations. It is necessary to study the electric field and its gradient along the tip axis and the substrate, respectively. In this paper, the 2D plane (xy planes) in the center of nanogap above the substrate is used to for the analysis of field distribution along the z axis (tip axis) and xy plane, since this two-dimensional plane is the detected region for Raman signals. For the field distribution along the z axis, electric field goes across this plane, and then we choose the field distribution projected on this plane.

Figure 5b is the electric field intensity at the center of the nano gap along tip axis. It is found that the strongest electric field intensity is focused within the circle with radius about 3 nm, and $|E|^2$ can reach up to $1.9 \times 10^5$. Figure 5c is the electric field gradient intensity along tip axis at the center of nano gap. It is found that the strongest electric field gradient are within the region of 1.5 nm < r < 5 nm. Figure 5d is the ratio of electric field gradient over electric field along the tip axis. It is found that the ratio is about 0.013 in atomic unit. Note that only the second term in Equation (1) is considered in above calculations. If the third term is also considered, the ratio should be about 0.026. Figure 5e is the electric field intensity at the center of nano gap along the substrate, and $|E|^2$ can reach up to $1.3 \times 10^3$, where the component of electric field intensity along the tip is excluded. It is found that the regions of the strongest electric field intensity are within 1.5 nm < r < 5 nm, but the electric field intensity is weak for r < 1.5 nm, as shown in Figure 5e. The changing tendency of electric field gradient along the substrate (see Figure 5f) is similar to that of the electric field gradient along the tip (see Figure 5c). Figure 5g is the ratio of electric field gradient over electric field, from which we can see that the ratio is about 1/10 in atomic unit. So, the most effective interval for the contribution of electric field gradient is within 1.5 nm < r < 5 nm. Note that only the second term in Equation (1) is considered in above calculations. If the third term is also considered, the ratio should be about 1/5. The electric field gradient along the tip axis can not be very accurate estimated, because the gap distance is too short within 1 nm. There is a better way to study the near field gradient Raman along the tip axis, using the Laplace's equation,

$$\frac{\partial E_{xx}}{\partial r_{xx}} + \frac{\partial E_{yy}}{\partial r_{yy}} + \frac{\partial E_{zz}}{\partial r_{zz}} = 0 \qquad (3)$$

We can see that the calculated Figure 5c is the same as Figure 5e, which revealed that the calculated Figure 5c is correct.

The first and the second terms in Equation (1) can be simplified according to the calculated electric dipole-dipole polarizability and electric dipole-quadruple polarizability (see section III in SI). From the intensities of electric field and electric field gradient in Figure 5b and c, the ratio of electric field gradient term (the second term plus the third term in Equation (1) over electric field term (the first term in Equation (1) is around 0.1. From the intensities of electric field and electric field gradient at the center 78 nm$^2$ area (except for the central 7.1 nm$^2$ region) in Figure 5e and f, the ratio of electric field gradient term (the second term in Equation (1) over electric field term (the first term in Equation (1) is around 1. So, after carefully assignments of the HV-TER spectrum along with Raman and IR spectra, we conclude that most of the strongly enhanced vibrational modes of HV-TERS were originated from the IR-active modes due to strong electric field gradient effect.

So, the qualitative palsmonic properties of TERS can be seen from Figure 1, according to above calculations in Figure 5. The electric field enhancement is strongest in the center of nanogap; while the electric field gradient enhancement at the center of the nanogap is weakest. When the tip apex is decreased, the ring of the strongest electric field gradient enhancement will be contracted towards to the center. If the condition is suitable enough, the strongest electric field enhancement and the strongest electric field gradient enhancement can be superposed at the center within several nanometers, and then we can obtain the optimal strongest Raman and IR-active mode enhancement at the same site near the center of nanogap.

### 2.3. The Connection between Theoretical Calculations and Experimental Results

The intensities of Raman (dipole Raman) and IR-active (multiple Raman) spectra in Figures 2 and 3 strongly are dependent on the first and second terms of Equation (1), respectively. The ratio of the intensity of multiple Raman over dipole Raman is dependent on the ratio of $\left(A_{\alpha\beta\gamma}\frac{\partial E_{\beta\gamma}}{\partial r}\right)/(\alpha_{\alpha\beta}E_{\beta})$. More detailed, $\left(\frac{\partial E_{\beta\gamma}}{\partial r}\right)/\left(E_{\beta}\right)$ and $\left(A_{\alpha\beta\gamma}\right)/\left(\alpha_{\alpha\beta}\right)$ are dependent on the palsmonic properties of TERS and the molecular property of polarizability, respectively. $\left(\frac{\partial E_{\beta\gamma}}{\partial r}\right)/\left(E_{\beta}\right)$ is the electric field gradient enhancement over electric enhancement, which were calculated by electromagnetic theory. $\left(A_{\alpha\beta\gamma}\right)/\left(\alpha_{\alpha\beta}\right)$ is determined by molecular properties, which can be calculated with quantum chemical method. Then the integrated ratio of intensity of IR-active modes over those of Raman can be obtained by $\left(\left(\frac{\partial E_{\beta\gamma}}{\partial r}\right)/\left(E_{\beta}\right)\right) \times \frac{A_{\alpha\beta\gamma}}{\alpha_{\alpha\beta}}$.

In our electromagnetic and quantum chemical calculations, the high-vacuum is not considered. The strong gradient effects have been revealed from above calculations. Also, strong gradient effect can also been observed in the SERS spectra in the system of Ag nanoparticle–Ag film at the ambient environment. So, the high vacuum is not an essential condition, but it can significantly enhance the ultrasensitive spectral signals, even at lower molecular concentration. As we know, the shorter distance between tip and substrate, the stronger electric field gradient effect can be obtained. Also, in all of kind TERS, the STM-based TERS is the best candidate for the shortest distance of nano gap than others. The high vacuum is needed for STM. Our system is STM-based TERS. So, our experiments were done in HV-TERS.

### 2.4. The Near-Field Gradient Effect on HV-TER Spectra at Low Frequency

We also measured the HV-TER spectrum of pyrazine adsorbed on Ag film, the Raman and the IR spectra of pyrazine powder at low frequency (see **Figure 6**). It is found that there are more strongly enhanced vibrational peaks in HV-TERS, compared to the Raman spectrum of pyrazine powder, which were contributed from the IR-active modes, by comparing with the IR spectrum of pyrazine powder. The assignments of Raman and IR spectra can be found in the literature.[26] There are five strongly enhanced IR-active modes in HV-TERS. Note that there is only one Fermi resonance peak at low frequencies.
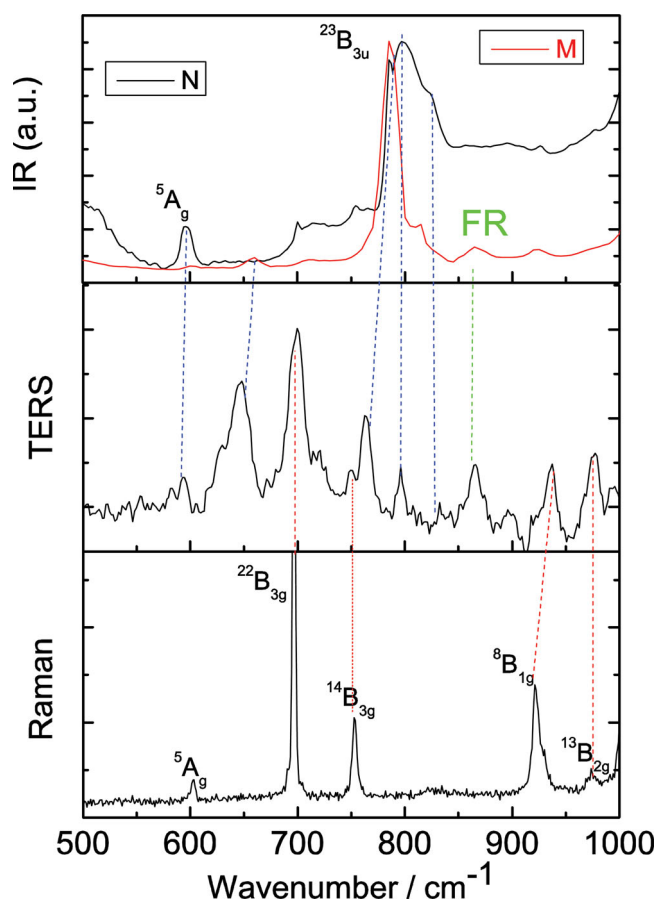


**Figure 6.** (a) The measured IR spectrum of pyrazine powder, (b) HV-TERS of pyrazine adsorbed on Ag film, and (c) Raman spectrum of pyrazine powder.

### 2.5. Gap Mode in TERS

The additional vibrational peaks in HV-TERS may also be interpreted by the gap-mode[5,33–37] in TERS, where the highly enhanced electromagnetic field being confined in the nanogap is used as an excitation source.[33] The emitted molecular Raman signals are further strongly enhanced by the tip, and then scattered into the far-field for measurements.[33,37] While the gap-mode TERS did not clearly point out weather the additional peaks in TERS are the Raman or IR active modes, i.e., the gap-mode TERS did not clearly reveal the selection rules for those additional vibrational peaks in TERS.

Our theoretical interpretation for the additional vibrational peaks in TERS, using electric field gradient effect, can not only provide rational interpretation for the additional vibrational peaks, but also can provide the selection rule for them. Usually, these additional vibrational modes are the nonlinear Raman, such as multipole Raman,[12,18] enhanced by the electric field gradient term in Equation (1).

## 3. Conclusion

We have experimentally in-situ observed the IR-active, Raman-active and the overtone modes of pyrazine adsorbed on Ag film simultaneously in HV-TERS. These unexpected "additional Raman modes" are attributed to molecular nonlinear vibrations and near field gradient effects. The high-vacuum can let us much easier observe the gradient effect or the nonlinear vibrations at lower molecular concentration, comparing with the SERS spectra at ambient environment. Theoretical calculations revealed that at the center of the nanogap within 20 $nm^2$ (along the substrate), the ratio of electric field gradient over electric field is about 1, which strongly supported the experimental results. The anomalous band intensity in Fermi resonance was also interpreted, where an overtone is stronger than the fundamental with which it is in resonance. These experimental findings can promote deep understanding in the unexpected "additional Raman peaks" in HV-TERS and provide a promising technique for ultrasensitive molecular spectroscopy.

## 4. Experimental Section

HV-TERS were measured with a home-built HV-TERS setup.[13] It consists of a homemade scanning tunneling microscope (STM) in a high vacuum chamber, a Raman spectrometer combined with a side illumination of 632.8 nm He-Ne laser light with an angle of 60° for Raman measurements, and three-dimensional piezo stages for the tip and sample manipulations. The laser power is 2 mW. The Raman optical system is collected in high vacuum by a stainless steel bellow valve, where a stainless steel tube was sealed inside the bellow with one end equipped with a quartz window to allow the light in and out of the high vacuum chamber, and the other end was equipped with a long working distance objective (NA = 0.5) to allow a highly efficient excitation and collection of weak Raman signals at the STM tip. The objective is in the high vacuum chamber, and the focus can be located in the nano gap in the tip-substrate junction. The outside of the bellow is fixed to the Raman probe equipped with a Notch filter to block the scattered light at the laser frequency. The Raman probe is mounted on a 3D adjuster equipped with piezo motor stages for optical fine-alignment. The pressure in the chamber is ~$10^{-7}$ Pa. A gold tip with

a ~50 nm diameter was made by electrochemical etching of a 0.25 mm diameter gold wire.[38] The substrate was prepared by evaporating a 100 nm Ag film to a newly cleared mica film under high vacuum. The film was immersed in a $1 \times 10^{-4}$ M pyrazine ethanol solution for 24 hours, and then washed with ethanol for 10 minutes to guarantee that there was only one monolayer of pyrazine molecules adsorbed on the Ag film. Then the sample was put into the high vacuum chamber immediately. The tunneling current and bias voltage are 1 nA and 1 V, respectively, in our experiment.

For comparison, the normal Raman scattering spectrum of pyrazine powder was measured with Renishaw inVia Raman system, and the laser with wavelengths of 632.8 nm is used, and the laser power is 2 mW. Furthermore, the IR vibrational spectrum of pyrazine powder was measured (the black curves in Figure 3 and Figure 5), using transmission mode of FTIR Excalibur 3100 spectrometer (Varian). The number of scans is 32 times, and the total acquisition time is 62 s.

The SERS spectra were also measured using the Renishaw inVia Raman system, and the laser with wavelengths of 632.8 nm is used, and the laser power is 2 mW. In the SERS measurements, the Ag nanoparticle–Ag film system is used for the comparison between TER spectra and SERS spectra, according to a recent experimental report.[28] The Ag film used is the same as that in HV-TERS, and the Ag nanoparticles were synthesized with Lee and Meisel method,[39] and the averaged radius size of Ag nanoparticles is 40 nm.[40] The Ag nanoparticles was immersed in a $1 \times 10^{-2}$ M pyrazine ethanol solution for 24 hours, and then doped on the Ag substrate. The SERS spectra were measured, after the sample was dried.

## Supporting Information

Supporting Information is available from the Wiley Online Library or from the author.

## Acknowledgements

[1] M. Stockle, Y. D. Suh, V. Deckert, R. Zenobi, *Chem. Phys. Lett.* **2000**, *318*, 131.

[2] N. Hayazawa, Y. Inouye, Z. Sekkat, S. Kawata, *Opt. Commun.* **2000**, *183*, 333.

[3] M. S. Anderson, *Appl. Phys. Lett.* **2000**, *4*, 3130.

[4] A. Hartschuh, E. J. Sanchez, X. S. Xie, L. Novotny, *Phys. Rev. Lett.* **2003**, *90*, 095503.

[5] B. Pettinger, B. Ren, G. Picardi, R. Schuster, G. Ertl, *Phys. Rev. Lett.* **2004**, *92*, 096101.

[6] J. Stadler, T. Schmid, R. Zenobi, *ACS Nano*, **2011**, *5*, 8442.

[7] E. Bailo, V. Deckert, *Angew. Chem. Int. Ed.* **2008**, *47*, 1658.

[8] J. Steidtner, B. Pettinger, *Phys. Rev. Lett.* **2008**, *100*, 236101.

[9] J. Stadler, T. Schmid, R. Zenobi, *Nanoscale* **2012**, *4*, 1856.

[10] J. Steidtner, B. Pettinger, *Rev. Sci. Instrum* **2007**, *78*, 103104.

[11] M. T. Sun, Y. R. Fang, Z. Y. Zhang, H. X. Xu, *Phys. Rev. E.* **2013**, *87*, 020401.

[12] N. Jiang, E. T. Foley, J. M. Klingsporn, M. D. Sonntag, N. A. Valley, J. A. Dieringer, T. Seideman, G. C. Schatz, M. C. Hersam, R. P. Van Duyne, *Nano Lett.* **2012**, *12*, 5061.

[13] M. T. Sun, Z. L. Zhang, H. R. Zheng, H. X. Xu, *Sci. Rep.* **2012**, *2*, 647.

[14] M. T. Sun, Z. L. Zhang, L. Chen, H. X. Xu, *Adv. Optical Mater.* **2013**, *1*, 449.

[15] A. Bouhelier, M. Beversluis, A. Hartschuh, L. Novotny, *Phys. Rev. Lett.* **2003**, *90*, 013903.

[16] S. J. Cyvin, J. E. Rauch, J. C. Decius, *J. Chem. Phys.* **1965**, *43*, 4083.

[17] K. Ikeda, Y. Saito, N. Hayazawa, S. Kawata, K. Uosaki, *Chem. Phys. Lett.* **2007**, *438*, 109.

[18] Z. L. Zhang, M. T. Sun, P. P. Ruan, H. R. Zheng, H. X. Xu, *Nanoscale* **2013**, *5*, 4151.

[19] A. D. Buckingham, *Adv. Chem. Phys.* **1967**, *12*, 107.

[20] E. Fermi, *Z. Phys.* **1931**, *71*, 250.

[21] R. A. Nyquist, H. A. Fouchea, G. A. Hoffman, D. L. Hasha, *Appl. Spectrsoc.* **1991**, *45*, 860.

[22] K. D. Bier, H. J. Jodi, *J. Chem. Phys.* **1987**, *86*, 4406.

[23] J. F. Bertran, L. Ballester, L. Dobrihalova, N. Sanchez, *Spectrochim. Acta A.* **1968**, *24*, 1765.

[24] B. T. Darling, D. M. Dennison, *Phys. Rev.* **1940**, *57*, 128.

[25] M. E. Kellman, *Annu. Rev. Phys. Chem.* **1995**, *46*, 395.

[26] K. V. Nechaev, P. M. Ei'kim, *J. Appl. Spectrosc.* **2005**, *72*, 9.

[27] S. E. Stein, in *NIST Chemistry Web Book, NIST Standard Reference Database Number 69* (Eds: P. J. Linstron, W. G. Mallard), National Institute of Standards and Technology Gaithersburg, MD **2003**, p.20899.

[28] Y. R. Fang, Y. Z. Huang, *Appl. Phys. Lett.* **2013**, *102*, 153108.

[29] B. Dong, Y. Fang, X. Chen, H. Xu, M. T. Sun, *Langmuir* **2011**, *27*, 10677.

[30] A. Kudelski, B. Pettinger, *Chem. Phys. Lett.* **2000**, *312*, 356.

[31] A. kudelski, *Chem. Phys. Lett.* **2006**, *427*, 206.

[32] a) A. M. Polubotko, *The Dipole-Quadrupole Theory of Surface Enhanced Raman Scattering*, Nova Science Publishers, New York **2009**; b) A. M. Polubotko, 2008, arXiv:0807.2936.

[33] J. Stadler, T. Schmid, R. Zenobi, *Nano Lett.* **2010**, *10*, 4514.

[34] J. Steidtner, B. Pettinger, *Phys. Rev. Lett.* **2008**, *100*, 236101.

[35] C. Blum, T. Schmid, L. Opilik, N. Metanis, S. Weidmann, R. Zenobi, *J. Phys. Chem. C.* **2012**, *116*, 23061.

[36] P. I. Geshev, K. Dickmann, *J. Opt. A: Pure Appl. Opt.* **2006**, *8*, S161.

[37] Y. Tanaka, A. Sanada, K. Sasaki, *Sci. Rep.* **2012**, *2*, 764.

[38] B. Ren, G. Picardi, B. Pettinger, *Rev. Sci. Instrum.* **2004**, *75*, 837.

[39] P. C. Lee, D. Meisel, *J. Phys. Chem.* **1982**, *86*, 3391.

[40] H. X. Xu, M. Kall, *ChemPhysChem* **2003**, *4*, 1001.

FULL PAPER